Stability Analysis in Homogeneous Charge Compression Ignition (HCCI) Engines With High Dilution

Chia-Jui Chiang and Anna G. Stefanopoulou, *Senior Member, IEEE*

***Abstract*—This paper analyzes the stability of the autoignition process of homogeneous charge compression ignition (HCCI) engines with exhaust dilution. We find conditions under which steady-state multiplicity exists with stable and unstable equilibria. This analysis is conducted taking into account the internal feedback structure of the thermal dynamics. Specifically, HCCI combustion timing determines the combustion heat produced and is determined by the heat provided through high internal exhaust gas recirculation from the previous combustion cycle. It is shown that the thermal equilibria are characterized by a simple returning map consisting of two curves, namely the breathing temperature curve and the combustion temperature curve. The influence of heat transfer and the cooling system in the system stability is also analyzed. The returning map and the stability of the multiple steady-state equilibria are confirmed with a high-order dynamic nonlinear model. The high-order dynamic model includes manifold filling and composition dynamics and has been validated both at steady state and during transient. It is shown that a static feedforward controller can cause instability during switching from a high to a low load. A dynamic feedforward controller, on the other hand, is able to stabilize the transition by reducing temperature excursions and, hence, keeping the temperature trajectories within stable regions.**

***Index Terms*—Feedforward control, heat transfer, homogeneous charge compression ignition (HCCI) engines, multiplicity, stability.**

NOMENCLATURE

Ah	Lumped parameter for convective area and coefficient.
C	Specific heat.
CA	Crankangle for a percentage of fuel burned.
EGR	Exhaust gas recirculation.
m	Mass (kg).
n	Polytropic constant.
N	Engine speed (r/min).
p	Pressure (Pa).
Q	Heat (Joule).
R	Gas constant (296.25 J/(kg-K)).
RBL	Rebreathing lift.
T	Temperature (K).
V	Volume (m^3).
W	Flow (kg/s).

Greek:

γ	Specific heat ratio.
θ	Crankangle.
$\Delta\theta$	Combustion duration.
τ	Engine cycle time (s).

Subscripts:

0	Ambient conditions.
1	Intake manifold conditions.
2	Exhaust manifold conditions.
ac	After combustion.
bc	Before combustion.
bd	Blowdown.
c	Cylinder conditions.
evo	Exhaust valve opening.
f	Fuel.
gw	Gas and wall.
im	Intake mass.
ivc	Intake valve closing.
LHV	Low heating value.
rbl	Rebreathed gas.
res	Residual.
SOC	Start of combustion.
w	Wall.

Manuscript received December 12, 2005. Manuscript received in final form August 7, 2006. Recommended by Associate Editor R. Rajamani. This work was supported by the National Science Foundation under Grant CMS-0201332.

The authors are with the Department of Mechanical Engineering, University of Michigan, Ann Arbor, MI 48109 USA (e-mail: cjchiang; annastef@umich.edu).

Color versions of Figs. 1, 2, 5–9, and 11–16 are available online at http://ieeexplore.ieee.org.

Digital Object Identifier 10.1109/TCST.2006.883333

I. INTRODUCTION

THE BASIS of homogeneous charge compression ignition (HCCI) engines is a fast and flameless combustion after an autoignition process of a homogeneous mixture. The autoignition in HCCI engines depends on a kinetically driven oxidation process [1] that does not rely on flame propagation [2]. The reactivity in an HCCI engine depends on the heat absorbed and the combustion is not followed by violent energy release typically characterized as knock [3]. Since the autoignition principle does not rely on flame propagation [2], it allows combustion in a homogeneous mixture similar to spark ignition (SI) engines. On the other hand, to achieve autoignition, HCCI engines require high compression ratios similar to compression ignition (CI) engines, and thus, achieve high thermal efficiency. In other words, the HCCI engine is a hybrid of the SI and CI engine concepts [4]. In fact, the HCCI engine integrates the advantages of both the CI and the SI engines [4]: 1) high fuel efficiency through high compression ratio and rapid heat release and 2) low NO_x and low particulate matter (PM) emissions due to low cylinder peak temperature (below 1700 K).

1063-6536/$25.00 © 2007 IEEE

Authorized licensed use limited to: IEEE Xplore. Downloaded on April 24, 2009 at 17:55 from IEEE Xplore. Restrictions apply.

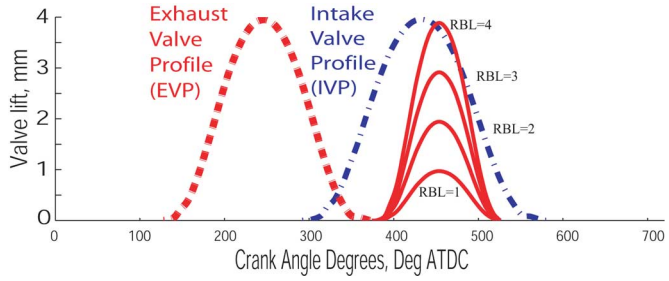

Fig. 1. Exhaust, intake, and rebreathing valve profiles.

The main difficulty in controlling HCCI combustion is that the ignition cannot be actuated directly. The autoignition timing of HCCI combustion is determined by the cylinder charge conditions, rather than the spark timing or the fuel injection timing that are used to initiate combustion in SI and CI engines, respectively [5]. Instead, controlled autoignition requires regulation of the charge properties, namely, temperature, pressure, and composition at the intake valve closing (IVC) as demonstrated by many experimental results [3], [6].

Many methods have been proposed to control HCCI combustion and exhaust gas recirculation (EGR) is found to be an affective actuation mechanism. Thring [6] found that HCCI is highly dependent on EGR rate and intake air temperature. After exploring the effects of several parameters on the ignition process and energy release of an HCCI engine based on experiment and simulation results, Najt *et al.* in [3] concluded that EGR primarily controls combustion by regulating temperatures. A sensitivity study in [7] also indicates that temperature is the dominant factor affecting the HCCI combustion timing when EGR is applied. HCCI combustion timing can, thus, be controlled by the regulation of charge temperature through recirculation of hot exhaust [5], [8]. One such method is a secondary opening of the exhaust valve during the intake stroke (rebreathing) [9]. The amount of dilution can be controlled by varying the lift of the secondary exhaust valve opening. We refer to this actuation as rebreathing lift (RBL) as shown in the valve profiles in Fig. 1. Using high dilution levels the exhaust gas heat can increase the charge temperature for the next cycle, and thus, determine the ignition and the exhaust temperature of the subsequent cycle [9], [10].

The HCCI engines can, thus, be viewed as chemical reactors such as continuous stirred tank reactors (CSTR) [3]. The multiplicity and stability of states in chemical reactors was widely studied in the 1950s [11], [12]. The start-up and asymptotic characteristics of chemical reactors can be analyzed with simple returning maps reported in the early 20th century by Liljenroth [13] and used more recently by Kantor in [14] for a potential explanation of the origin of cycle-to-cycle variability in SI engines. The autoignition equilibria in HCCI engines and their stability can be described by a returning map that captures the temperature effect of the prior combustion on the next cycle via the exhaust gas recirculation, as we will show in this paper.

In the combustion and automotive literature there are many citations about the stability of HCCI combustion and especially the dynamic connection between subsequent combustion cycles during transients. For example, in [15] the authors stress the importance of taking into account the combustion of the previous cycle. Due to the large amount of residuals (or internal exhaust gas recirculation) a combustion event depends largely on the chemical and thermal state of the prior combustion cycle. In [16], the authors demonstrate cyclic fluctuations in HCCI combustion based on an engine cycle model with thermal and chemical coupling, for an operating point corresponding to very high external EGR and lean air-fuel ratio. There is strong evidence that partially oxidized fuel from misfiring cycles can affect the ignition of the charge in the next cycle [17] leading to limit cycles. The importance of the composition effect on HCCI combustion really depends on the operating conditions and structure of the engines as several papers have suggested: 1) Najt *et al.* in [3] observe from experiment that exhaust gas recirculation mainly affects HCCI combustion through temperature and chemistry effect is negligible; 2) in [7], we analyze the sensitivity of the combustion timing and duration with respect to factors such as temperature, pressure, fuel, and oxygen concentration at operating points in a HCCI engine with high residual and find that composition effect is negligible compared with temperature; and 3) Caton *et al.* in [18] find that in an HCCI engine with high heat loss in the cylinder, cylinder temperature does not change much despite increased hot exhaust gas and, thus, composition becomes important. In this paper, we neglect the chemical energy coupling. We, instead, assume fully burnt fuel and concentrate on the cycle-to-cycle coupling introduced by the thermal energy of the residuals.

In this paper, we follow the work on stability of autothermal chemical reactors [11], [19], [20], and use the mean value model (MVM) [9], which relies on the average values of cylinder flows in each cycle, to find the thermal equilibria of an HCCI engine with high residuals. By assuming fast manifold dynamics and accurate air-to-fuel ratio control, the temperature dynamics constitute the dominant and slow dynamics of the overall system. Specifically, the charge temperature in the cylinder at intake valve closing, $T_{\rm ivc}$, and the blow down temperature, $T_{\rm bd}$, are the two cycle-to-cycle interacting variables that define the HCCI combustion process. The cycle-to-cycle coupling of the temperature dynamics, thus, determines the stability of the open-loop HCCI dynamics. Specifically, $|(\partial T_{\rm bd}/\partial T_{\rm ivc})(\partial T_{\rm ivc}/\partial T_{\rm bd})| < 1$ causes a passive system associated with negative feedback and, thus, contributes to the stability of the system. Furthermore, to analyze the effect of heat transfer in the exhaust manifold on the open-loop stability of an HCCI engine, the exhaust runner heat transfer model is added to the mean value model (MVM) in [9]. This modified model is validated with transient experimental data.

Our results corroborate many combustion stability results in the combustion literature based on experiment data. For example, Willand *et al.* [1] claimed that "Late combustion provides hot exhaust gas causing the next cycle to ignite earlier and reduce exhaust gas temperature again." In other words, the timing of start of combustion (SOC) controlled internally through the retained exhaust gas, also known as internal EGR (iEGR), is self-stabilizing and, thus, more robust. Also, Thring [6] explored the operating limits of an HCCI engine by varying EGR and AFR. He observed that "…deep in the knock zone, knock could become excessively heavy, and engine combustion

Authorized licensed use limited to: IEEE Xplore. Downloaded on April 24, 2009 at 17:55 from IEEE Xplore. Restrictions apply.

timing would become more and more advanced until the engine would finally stop firing altogether." More recently, Olsson *et al.* [4] discovered by experiments that "The energy exchange or storage can drive the combustion event to instability… While in some cases operation is stable and very easy to control, other operating conditions require fast and accurate feedback control to maintain steady state operation." Although many experiments have been performed to design HCCI engines and develop steady-state operating maps, no stability analysis has been done to support or explain the experimentally observed dynamic behavior reported in [1], [4], and [6]. Our work fills this gap by offering analytical basis for understanding the HCCI engine autoignition dynamics with high dilution.

Specifically, we found that the thermal dynamics are described by a unique stable thermal equilibrium, if the wall temperature (T_w) of the exhaust runners and exhaust manifold are perfectly controlled with an active cooling system. On the other hand, insulated exhaust runners and exhaust manifold sustain the thermal energy of the recycled gases and may enhance cycle-to-cycle temperature growth under early-ignition conditions, as explained in this paper and observed in the experiments [4] and [6].

In Section II the HCCI engine model that is used in our analysis is summarized. Specifically, in Section II-A the system dynamics are revisited to include the exhaust manifold temperature dynamic so as to capture the heat transfer effect on the open-loop stability. In Section II-B and II-C, the combustion and breathing characteristics are presented. These characteristics constitute the feedback loop between the two interacting temperature variables. The model in Section II is then validated with transient experiment data in Section III. In Section IV, the steady-state temperature returning maps are shown and the multiplicity and stability of the equilibria are explained. In Section V the open-loop and controlled temperature trajectories are shown. We present in Section V-B a dynamic feedforward controller which is able to stabilize the transition by reducing temperature excursions and, hence, keeping the temperature trajectories within stable regions.

II. Engine Model

A summary of the HCCI engine model dynamics is presented in this section. The mean value model (MVM) from [9] is extended by accounting for the heat losses in the exhaust manifold. This extension allows us to study the effect of heat transfer on the multiplicity and stability of the temperature equilibria. The burned gas compositions are neglected in this model since the combustion timing of a high residual HCCI engine is dominated by charge temperature [3], [6], [7]. The system dynamics include three (3) continuous and two (2) discrete in-time states, described in Section II-A.

Fig. 2 shows the schematic diagram associated with the engine model. There are three relevant volumes: 1) the intake manifold denoted with subscript 1; 2) the exhaust manifold denoted with subscript 2; and 3) the cylinder denoted with subscript c. The atmospheric conditions are denoted with subscript 0. In each volume, volumes are denoted with V, pressures with p, temperatures with T, and masses with m. The rate of the flow from volume x to volume y is denoted as W_{xy} and is calculated based on the orifice flow equation [21, App. C].

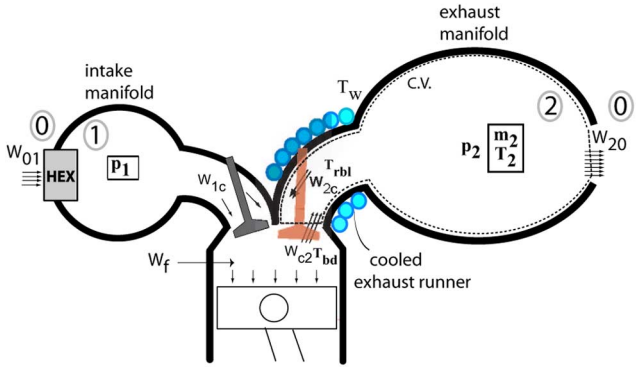

Fig. 2. Schematic diagram of the engine.

A. System Dynamics

A heat exchanger (HEX) keeps the intake manifold at isothermal conditions, $T_1 = 90\,^{\circ}\mathrm{C}\,(363\,\mathrm{K})$. Therefore, one continuous state is sufficient to characterize the intake manifold, namely, the spatially average intake manifold pressure p_1, which is determined through the conservation of the mass in the intake manifold and the ideal gas law

$$\dot{p}_1 = \frac{RT_1(W_{01} - W_{1c})}{V_1} \tag{1}$$

where R is the gas constant. Since the engine is intended to run unthrottled, we anticipate small backflows through the orifices 01 and 20. For most conditions, however, the manifold pressures satisfy $p_1 < p_0 < p_2$ so that all the flows through the valves and orifices are due to the pressure difference between the volumes. The flow from the intake manifold to the cylinder W_{1c} is a forced flow due to cylinder pumping and has been characterized in [9] using experimental data as a function of p_1, p_2 and the rebreathing lift (RBL). Similarly, the rebreathing flow W_{2c} has been characterized in [9] as a function of p_1, p_2, RBL, and the rebreathed flow temperature T_{rbl} discussed as follows.

The two other continuous states are in the exhaust manifold. One of them is given by the conservation of mass in the control volume containing the exhaust runner and exhaust manifold (C.V. in Fig. 2)

$$\dot{m}_2 = W_{c2} - W_{20} - W_{2c}. \tag{2}$$

The energy balance equation in the exhaust control volume C.V. includes the heat transferred to the wall. The heat transfer is captured through a lumped constant parameter of the convective area and the convection coefficient between the gas in the exhaust manifold and wall $Ah_{\mathrm{gw}} = 2.5$ W/K. We consider the exhaust manifold wall temperature T_w as constant at 400 K after assuming a perfect cooling system. The gas constant R, specific heat C_p (at constant pressure), and C_v (at constant volume), and thus, specific heat ratio γ, are all assumed to be constant. The conservation of energy gives the final continuous state

$$\dot{T}_2 = \frac{1}{C_v m_2}\left[C_p W_{c2} T_{\mathrm{bd}}^{d} - \left(C_v W_{c2} + R(W_{2c} + W_{20})\right) \times T_2 - Ah_{\mathrm{gw}}(T_2 - T_w)\right] \tag{3}$$

Authorized licensed use limited to: IEEE Xplore. Downloaded on April 24, 2009 at 17:55 from IEEE Xplore. Restrictions apply.

where $T_{\rm bd}^d$ is the delayed temperature of the blowdown gas entering the exhaust runner. The ideal gas law can then be used to calculate the pressure in the exhaust manifold: $p_2 = Rm_2T_2/V_2$.

Two discrete-in-time states are introduced due to the cycle-delay $\tau = N/120$, where N is the engine speed (rev/min). Specifically, the flow and temperature of the gas exiting the cylinder are both delayed

$$W_{c2}(t+\tau) = W_{1c}(t) + W_f(t) + W_{2c}(t) \tag{4}$$
$$T_{\rm bd}^d(t+\tau) = T_{\rm bd}(t) \tag{5}$$

where W_f is the fuel mass flow injected, and $T_{\rm bd}$ is the temperature of the blowdown gas in the previous cycle. The blowdown gas temperature $T_{\rm bd}$ is calculated in the last phase of the combustion model, presented in Section II-B.

Hence, the only other differences between the model with insulated exhaust runner in [9] and the one with heat transfer presented here, are 1) the spatially averaged exhaust manifold temperature T_2 in (3), which depends on the heat transferred to the wall, and 2) the rebreathed gas temperature $T_{\rm rbl}$, which is an elevated exhaust gas temperature T_2 by ΔT_w due to the heat transfer between the exhaust runner walls and the rebreathed gas that moves from the exhaust manifold back into the cylinder

$$T_{\rm rbl} = T_2 + \Delta T_w. \tag{6}$$

B. Combustion ($T_{\rm ivc} \rightarrow T_{\rm bd}$)

The combustion model in [9] is revisited in this section. The blowdown temperature $T_{\rm bd}$ is determined by the charge temperature and intake and exhaust manifold pressure ($T_{\rm ivc}$, p_1, and p_2) using an Arrhenius integral for the ignition timing $\theta_{\rm SOC}$ [22] and a instantaneous temperature rise ΔT at the end of combustion θ_c based on [14]. The combustion model development and steady-state validation at 7 to 12 mg/cycle fueling rates, 1.5 to 4 mm RBL values is shown in [9]. We briefly summarize the equations below to be used in the calculation of the combustion characteristic $T_{\rm bd} = f_c(T_{\rm ivc})$ shown as follows.

The ignition timing $\theta_{\rm SOC}$ which corresponds to crankangle for 1% fuel burned (CA_{01}) is calculated by:

$$\int_{\theta_{\rm ivc}}^{\theta_{\rm soc}} A p_{\rm ivc}^n v_{\rm ivc}^{n_c n}(\vartheta) \exp\left(-\frac{E_a v_{\rm ivc}^{1-n_c}(\vartheta)}{RT_{\rm ivc}}\right) d\vartheta = 1$$

where $v_x(\vartheta_y) = \dfrac{V_c(\vartheta_x)}{V_c(\vartheta_y)}$

hence $T_{\rm soc} = T_{\rm ivc} v_{\rm ivc}^{(n_c-1)}(\theta_{\rm soc})$.

The end of combustion $\theta_c = CA_{90} = \theta_{\rm soc} + \Delta\theta$

and $CA_{50} = \theta_{\rm soc} + 0.55\Delta\theta$

where $\Delta\theta = k(T_{\rm soc})^{(-2/3)}(T_m)^{1/3} \exp\left(\dfrac{E_c}{3R_u T_m}\right)$,

$$T_m = T_{\rm soc} + e\Delta T,$$
$$\Delta T = \left(\frac{R}{(C_v V_{\rm ivc})}\right)\left(\frac{Q_{LHV} m_f T_{\rm ivc}}{p_{\rm ivc}}\right),$$
$$e = a_0 + a_1 k, \text{ and } k = b_0 + b_1\theta_{\rm soc} + b_2\theta_{\rm soc}^2.$$

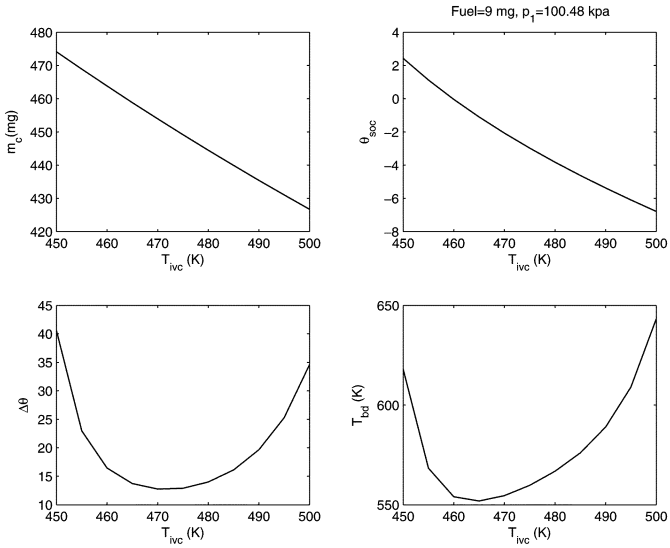

Fig. 3. Combustion characteristics: the intermediate variables for a fixed fuel flow rate at 9 mg/cycle and p_1 at 100.48 kPa.

The cylinder temperatures and pressures are then calculated:

before combustion $T_{\rm bc} = T_{\rm ivc} v_{\rm ivc}^{(n_c-1)}(\theta_c)$, $p_{\rm bc} = p_{\rm ivc} v_{\rm ivc}^{n_c}(\theta_c)$

after combustion $T_{\rm ac} = T_{\rm bc} + \Delta T$, $p_{\rm ac} = p_{\rm bc}\left(\dfrac{T_{\rm ac}}{T_{\rm bc}}\right)$

at exhaust valve opening

$$T_{\rm evo} = T_{\rm ac} v_c^{(n_e-1)}(\theta_{\rm evo}) \text{ and } p_{\rm evo} = p_{\rm ac} v_c^{n_e}(\theta_{\rm evo}),$$

and finally, the blowdown $T_{\rm bd} = T_{\rm evo}\left(\dfrac{p_2}{p_{\rm evo}}\right)^{n_e - 1/n_e} + \Delta T_{\rm bd}$. (7)

Fig. 3 shows some of the intermediate variables during the combustion process. When $T_{\rm ivc}$ increases, the trapped charge m_c, drops (due to the ideal gas law), and the combustion starts earlier (the advanced $\theta_{\rm soc}$ is predicted by the Arrhenius integral). The dependency of the combustion duration $\Delta\theta$ on $\theta_{\rm soc}$ leads to a parabolic shape of combustion duration. A nonmonotonic relation between the combustion duration and $\theta_{\rm soc}$ is also presented in [23] and [24]. The main reason for this nonmonotonic behavior is not well understood. The authors in [23] argued that this nonmonotonic behavior comes from the effect of the recycled burned gas. A nonmonotonic relation between the burn duration and start of combustion timing, however, also appears in [24] when intake temperature (not exhaust gas recirculation) is used to control the combustion timing. It is also shown in [7] that a combustion duration model containing the fuel and oxygen fraction cannot match the nonmonotonic behavior in the test data and a parabolic parameter e is necessary to capture the combustion efficiency and heat loss. The parabolic shape of $\Delta\theta$ together with the parabolic shape of the volume ratio $v_x(\theta_y)$ in (7) around the top dead center (TDC) results in a nonmonotonic behavior of $T_{\rm bd}$ as $T_{\rm ivc}$ increases. Note here that an increase in $T_{\rm ivc}$ can occur during an increase in RBL or after an increase in the rebreathed gas temperature $T_{\rm rbl}$ as shown in Section II-C. The dependency of $T_{\rm bd}$ on $T_{\rm ivc}$, which in turn depends on the previous $T_{\rm bd}$, constitutes the feedback loop, shown in Fig. 4, that we analyze in this paper.

Authorized licensed use limited to: IEEE Xplore. Downloaded on April 24, 2009 at 17:55 from IEEE Xplore. Restrictions apply.

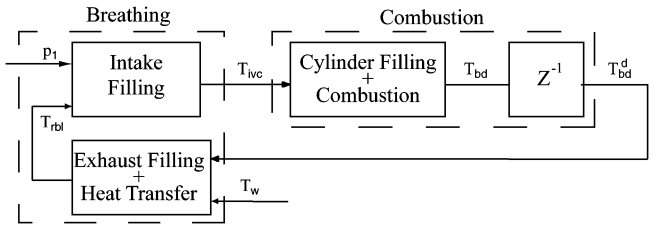

Fig. 4. Thermal feedback constituted by the breathing characteristics (including heat transfer in the exhaust runner) and the combustion characteristics of the HCCI engine with large percentage of residual gas in the cylinder charge.

C. *Breathing* ($T_{\rm bd} \rightarrow T_{\rm rbl} \rightarrow T_{\rm ivc}$)

In this section, we construct the steady-state characteristics of the breathing block in Fig. 4, which maps the blowdown temperature $T_{\rm bd}$ to intake charge temperature $T_{\rm ivc}$ through the rebreathed flow temperature $T_{\rm rbl}$.

The charge temperature at IVC is approximated as the weighted temperature of the mixing gas mass from the intake manifold ($T_1 m_{\rm im}$) and the reabreathed flow ($T_{\rm rbl} m_{\rm res}$)

$$T_{\rm ivc} = \frac{T_1 m_{\rm im} + T_{\rm rbl} m_{\rm res}}{m_{\rm im} + m_{\rm res}} \tag{8}$$

where the cylinder mass associated with the flow from the intake manifold to the cylinder $m_{\rm im}$ during a period of cycle τ is given at steady state by

$$m_{\rm im} = W_{1c}\tau = W_{01}\tau. \tag{9}$$

The mass of gas from the rebreathing flow $m_{\rm res}$, also called residual mass, is calculated based on the ideal gas law and Dalton's law of the partial pressures of the gas from the intake manifold $p_{\rm im}$, and the gas from the rebreathing flow $p_{\rm res}$, as they contribute to the total in-cylinder pressure at IVC $(p_{\rm ivc})$

$$\begin{aligned} m_{\rm res} &= \frac{p_{\rm res} V_{\rm ivc}}{R T_{\rm rbl}} = \frac{(p_{\rm ivc} - p_{\rm im}) V_{\rm ivc}}{R T_{\rm rbl}} \\ &= \frac{p_{\rm ivc} V_{\rm ivc}}{R T_{\rm rbl}} - m_{\rm im} \frac{T_1}{T_{\rm rbl}} \\ &= \frac{p_{\rm ivc} V_{\rm ivc}}{R T_{\rm rbl}} - W_{01}\tau \frac{T_1}{T_{\rm rbl}}. \end{aligned} \tag{10}$$

The in-cylinder pressure at IVC $p_{\rm ivc}$, is approximated well as a linear function of the intake manifold pressure p_1 using experimental data [9]

$$p_{\rm ivc} = \beta_0 + \beta_1 p_1. \tag{11}$$

By substituting (9)–(11) into (8) we obtain the expression for the steady-state temperature in the cylinder at intake valve closing, $T_{\rm ivc}$ as

$$T_{\rm ivc} = \frac{(\beta_0 + \beta_1 p_1) V_{\rm ivc} T_{\rm rbl}}{W_{01}\tau R (T_{\rm rbl} - T_1) + (\beta_0 + \beta_1 p_1) V_{\rm ivc}}. \tag{12}$$

The temperature of the rebreathed gas $T_{\rm rbl}$, in turn, is a function of the mean temperature of the gas in the exhaust manifold T_2, from (6). At steady state, based on (3), T_2 is a function of $T_{\rm bd}$ and the wall temperature T_w

$$T_2 = \frac{C_p W_{c2} T_{\rm bd} + A h_{\rm gw} T_w}{C_p W_{c2} + A h_{\rm gw}}. \tag{13}$$

Combining (6) with (13) results in

$$T_{\rm rbl} = \frac{C_p W_{c2}}{C_p W_{c2} + A h_{\rm gw}} T_{\rm bd} + \frac{A h_{\rm gw}}{C_p W_{c2} + A h_{\rm gw}} T_w + \Delta T_w \tag{14}$$

which can be written in a compact way as

$$T_{\rm rbl} = \alpha_{\rm ht} T_{\rm bd} + (1 - \alpha_{\rm ht}) T_w + \Delta T_w. \tag{15}$$

The ratio $\alpha_{\rm ht}$ weighs the heat gained from the blowdown gases versus the heat lost to the wall. If there is no heat loss to the wall, then $\alpha_{\rm ht} = 1$, $\Delta T_w = 0$, and $T_{\rm rbl} = T_{\rm bd}$ as in the case of insulated walls in [25]. In all other cases, $\alpha_{\rm ht} < 1$, which weakens the thermal coupling ($T_{\rm bd} \rightarrow T_2 \rightarrow T_{\rm rbl} \rightarrow T_{\rm ivc} \rightarrow$ new $T_{\rm bd}$) from cycle-to-cycle.

Typical values of the parameters can be used to illustrate how heat transfer affects the slope of the breathing temperature curve. For example, by using $A h_{\rm gw} = 2.5$ W/K, $C_p = 1.0369$ kJ/(kg- K), $W_{c2} = 3.8$ g/s and $\Delta T_w = 35$ in (14), the temperature of the rebreathing flow becomes

$$T_{\rm rbl} = 0.6 T_{\rm bd} + 0.4 T_w + 35. \tag{16}$$

Compared with the case when the exhaust manifold is insulated $T_{\rm rbl} = T_{\rm bd}$, the resulting steady state slope from $T_{\rm bd}$ to $T_{\rm rbl}$ in (16) is reduced by 40%. Thus, by substituting (16) into (12), the slope of the steady-state temperature curve from $T_{\rm bd}$ to $T_{\rm ivc}$ is also reduced. Specifically, the steady-state gain from $T_{\rm bd}$ to $T_{\rm ivc}$ decreases when a higher heat transfer rate is applied (increased $A h_{\rm gw}$).

III. Experimental Validation During Transients

Experimental data during step changes in fuel and RBL (independently) for a single-cylinder gasoline HCCI engine were provided for validation by General Motors Company after the engine (cylinder head) was modified from the original engine that was used to develop the model. Due to the differences between the engines used for model calibration versus validation, an offset between the experiment and simulation is observed. To facilitate the comparison between the predicted and the measured values and demonstrate that the dynamic model captures the transient cycle-to-cycle behavior, two vertical axes will be used for the validation figure in this section. The left axis shows the measured values, whereas the right axis shows the predicted values.

The validation data were provided at a fixed rate with 0.05 s sampling time after downsampling from a sampling time of 0.005 s. At 1000 r/min, the fixed sampling time of 0.05 s corresponds to at least two samples per cycle. Hence, the values of the crankangle of 50% fuel burned (CA_{50}) values capture cycle-to-cycle variability. The two experiments were performed in two different periods (one month apart). The exhaust runner temperature measurement is important for validating and unraveling the thermal coupling by the rebreathed flow. For the validation, we augment associated sensor dynamics in the rebreathed gas temperature $T_{\rm rbl}$ of our model to compare with the

Authorized licensed use limited to: IEEE Xplore. Downloaded on April 24, 2009 at 17:55 from IEEE Xplore. Restrictions apply.

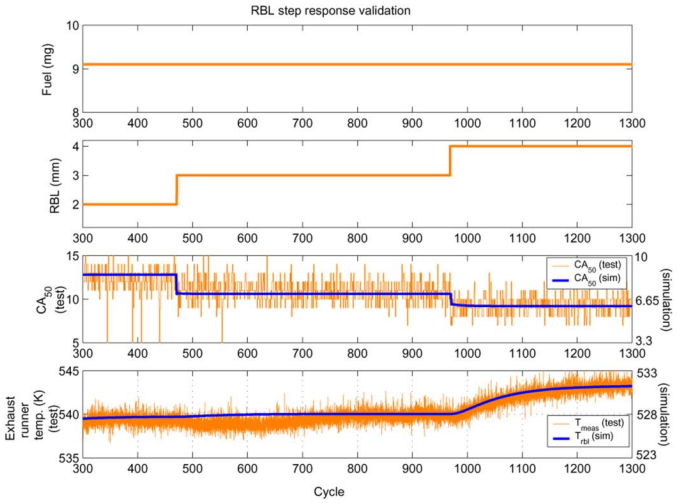

Fig. 5. Rebreathing lift step response validation.

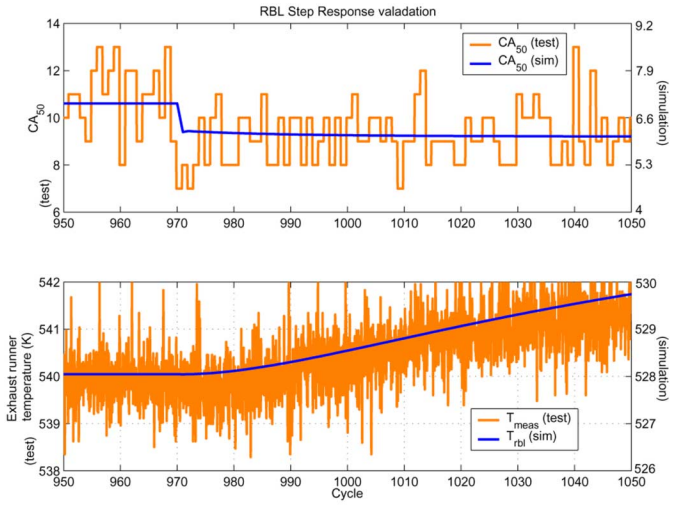

Fig. 6. Zoomed view of Fig. 5.

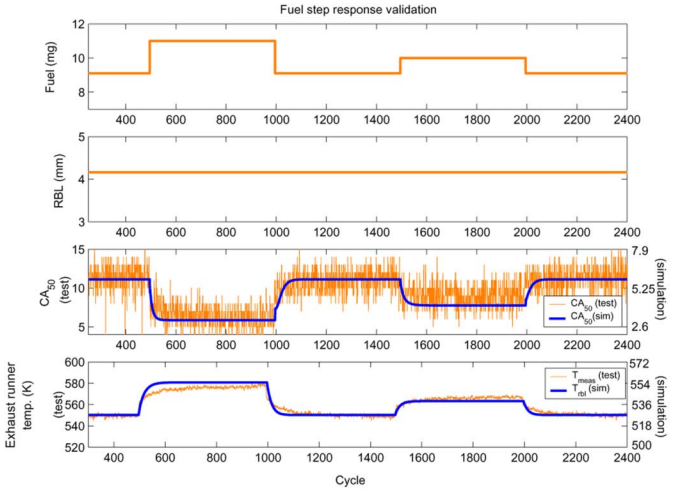

Fig. 7. Fuel step response validation.

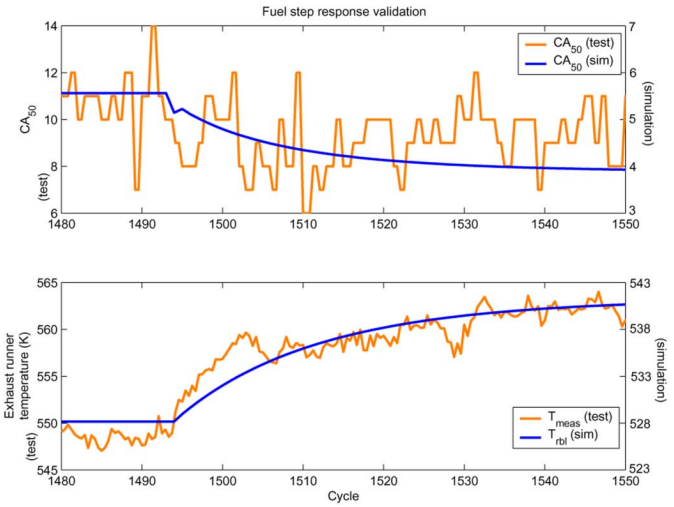

Fig. 8. Zoomed view of Fig. 7.

measured temperature $T_{\rm meas}$. A slow thermocouple with time constant 2.4 s (20 cycles at 1000 r/min) was used for the exhaust runner temperature during the RBL step. The experiment with the fuel step was performed with a fast thermocouple at the exhaust runner.

The transient response during RBL steps and fuel steps are shown in Figs. 5 and 7, respectively, with zoomed-in views shown in Figs. 6 and 8. The figures show that CA_{50} is advanced when either RBL or fuel increases. The measured temperature at the exhaust runners $T_{\rm meas}$, shown in the last subplot of Figs. 5–7 is the rebreathed gas temperature $T_{\rm rbl}$, modified by the sensor dynamics if any. Fig. 5 shows that the measured temperature $T_{\rm meas}$ increases more in the second RBL step change (from 3 mm to 4 mm) than in the first one (from 2 to 3 mm). This nonlinear behavior between RBL and $T_{\rm meas}(T_{\rm rbl})$ is predicted by our combustion model. Specifically, the rebreathed gas temperature $T_{\rm rbl}$ (15) depends on the nonmonotonic behavior of $T_{\rm bd}$ as $T_{\rm ivc}$ is increased through RBL. The implication of this nonlinear behavior to the thermal stability of an HCCI engine was first reported in [25] and is further studied in this paper.

IV. Global Steady-State Temperature Equilibria

Assuming that the temperature dynamics dominate the engine behavior, we analyze the global temperature equilibria using a return map consisting of two processes discussed as follows.

1) The breathing process includes the intake and exhaust manifold filling dynamics as gases are drawn from both manifolds during the rebreathing event $T_{\rm bd} \rightarrow T_{\rm rbl} \rightarrow T_{\rm ivc}$.
2) The combustion process provides the charge temperature after the blowdown process $T_{\rm bd}$ as it is governed by the combustion following the autoignition of the compressed charge $T_{\rm ivc} \rightarrow T_{\rm bd}$.

The internal temperature feedback shown schematically in Fig. 4 exists in a small percentage in conventional SI or CI engines, but its effects are pronounced in HCCI engines due to the large percentage of residual gas in the cylinder charge.[1]

To get the exact mapping from $T_{\rm bd}$ to $T_{\rm ivc}$ (breathing) and from $T_{\rm ivc}$ to $T_{\rm bd}$ (combustion), the exact manifold pressures need to be determined for fixed fueling and RBL. To resolve the

[1]Up to 60% dilution is achieved during the rebreathing valve event at RBL = 4 mm, $W_f = 75$ mg/s (9 mg/cycle), and $p_1 = 100.48$ kPa.

Authorized licensed use limited to: IEEE Xplore. Downloaded on April 24, 2009 at 17:55 from IEEE Xplore. Restrictions apply.

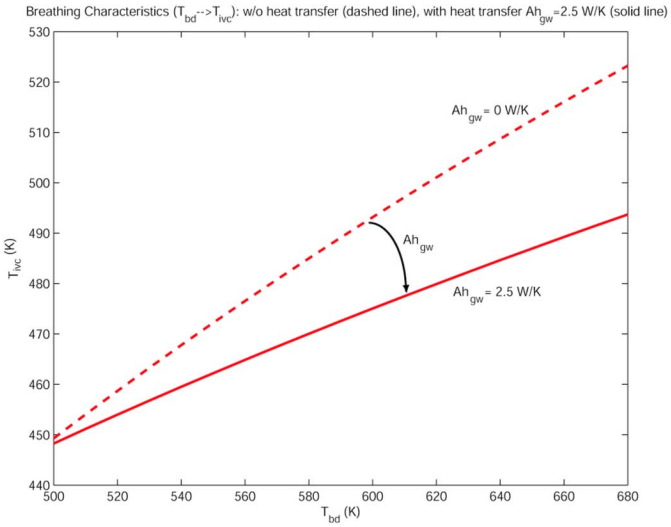

Fig. 9. Breathing characteristics: $T_{\rm ivc} = f_b(T_{\rm bd})$ for fuel flow rate fixed at 9 mg/cycle, RBL at 4 mm, and intake manifold pressure p_1 at 100.48 kPa. The addition of heat transfer in the exhaust manifold ($Ah_{\rm gw} = 2.5\ {\rm W/K}$) changes the slope of the breathing curve.

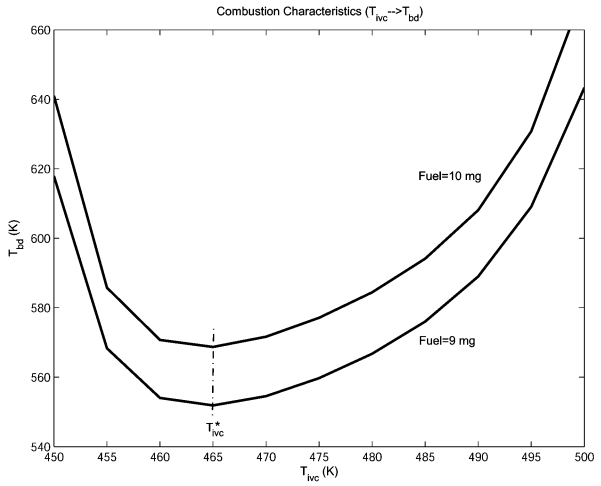

Fig. 10. Combustion characteristics: $T_{\rm bd} = f_c(T_{\rm ivc})$ for fuel flow rate at 9 and 10 mg/cycle and intake manifold pressure p_1 at 100.28 kPa.

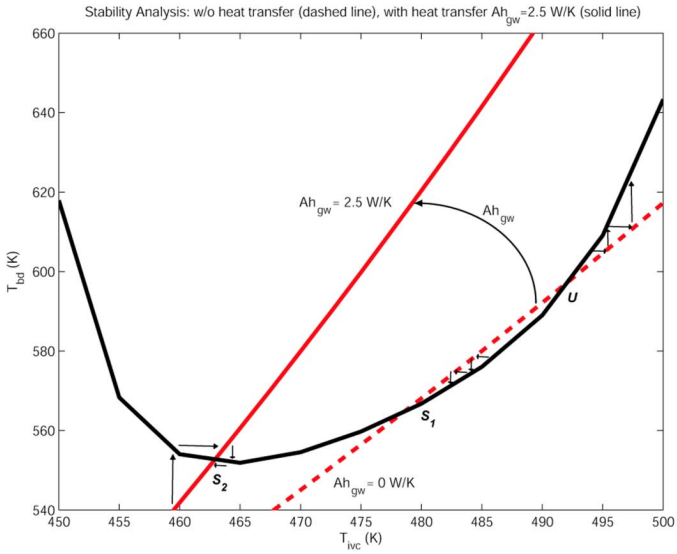

Fig. 11. Stability analysis through the recursive mapping between $T_{\rm ivc}$ and $T_{\rm bd}$ for fuel flow rate fixed at 9 mg/cycle.

coupling, the steady-state equations are programmed and solved using the symbolic manipulations in Matlab. Specifically, the temperature equations used are as follows:

- equation (7) for $T_{\rm bd} = F_c(T_{\rm ivc}, p_1, p_2, W_f)$;
- equation (14) for $T_{\rm rbl} = F_{b1}(T_{\rm bd}, p_1, p_2, {\rm RBL})$;
- equation (12) for $T_{\rm ivc} = F_{b2}(T_{\rm rbl}, p_1)$;

and mass flow rate equations are as follows:

- $W_{1c}(p_1, p_2, {\rm RBL}) = W_{01}(p_1)$;
- $W_{20}(p_2, T_2) = W_{01}(p_1) + W_f$;
- $W_{c2} = W_{01}(p_1) + W_{2c}(p_1, p_2, T_{\rm rbl}, {\rm RBL}) + W_f$.

Note here that the flows depend on the temperatures and so the steady-state temperature and flow equations need to be solved simultaneously.

The breathing characteristics mapping from $T_{\rm bd}$ to $T_{\rm ivc}$ is shown in Fig. 9 for a fixed-fuel flow rate at 9 mg/cycle, RBL at 4 mm, and intake manifold pressure p_1 at 100.48 kPa. The addition of heat transfer in the exhaust manifold ($Ah_{\rm gw} = 2.5\ {\rm W/K}$) changes the slope of the curve, a change which is critical to the steady-state mapping.

Similar to Fig. 3 (lower right plot), the combustion characteristics mapping from $T_{\rm ivc}$ to $T_{\rm bd}$ is shown in Fig. 10 for fuel flow rate at 9 and 10 mg/cycle and intake manifold pressure p_1 at 100.48 kPa. The curve shifts upward when the fuel flow rate increases. It is obvious from Fig. 10 that there is a fuel-optimum $T^*_{\rm ivc}$ for which most of the chemical energy of the fuel is converted to useful mechanical work and not exhaust gas heat. In other words, $T_{\rm ivc}$ determines combustion timing in the HCCI engine and, thus, affects the thermal efficiency. It is also anticipated that the magnitude of the slope $|\partial T_{\rm bd}/\partial T_{\rm ivc}|$ to the right of $T^*_{\rm ivc}$ (very advanced combustion timing) will be smaller than the one to the left of $T^*_{\rm ivc}$ (less advanced combustion timing). This difference in slopes could be more pronounced depending on the heat dissipated through the walls during early combustion.

To obtain a graphical representation of the HCCI engine temperature equilibria, we switch the axes in Fig. 9 to superimpose the breathing temperature curves (straight lines) together with the combustion temperature curve ("U" shape) in Fig. 11. The breathing temperature curve provides the cylinder charge temperature at IVC of the next cycle $T_{\rm ivc}(k+1) = f_b(T_{\rm bd}(k))$, as it is governed by the breathing characteristics (with heat transfer in the exhaust manifold) of the engine. The combustion temperature curve provides the blowdown temperature of cycle k, $T_{\rm bd}(k) = f_c(T_{\rm ivc}(k))$, as it is governed by the combustion following the autoignition of the compressed charge. The intersection of the breathing curve (straight line) and the combustion curve ("U" shape) defines a temperature equilibrium point.

The stability of an equilibrium point for the recursive mapping is determined by the slopes of the two curves near the intersection. We conclude that stable equilibria exists when $|(\partial T_{\rm bd}/\partial T_{\rm ivc})(\partial T_{\rm ivc}/\partial T_{\rm bd})| < 1$. Basically, the equilibrium is stable around the lowest point on the combustion curve ($T_{\rm bd}$ at 550 K; $T_{\rm ivc}$ at 465 K). On the other hand, unstable equilibrium points appear when the two curves have two intersections, as

Authorized licensed use limited to: IEEE Xplore. Downloaded on April 24, 2009 at 17:55 from IEEE Xplore. Restrictions apply.

with the dotted line in the right portion of Fig. 11. Recall that this dotted line corresponds to the breathing characteristics of an engine with an insulated exhaust manifold ($Ah_{\rm gw} = 0\,{\rm W/K}$). When RBL is 4 mm and p_1 is equal to 100.48 kPa, one of the intersections of the breathing and combustion curves is a stable equilibrium point. The stability of this equilibrium can be confirmed by following the temperature converging sequence after a small perturbation from the equilibrium point S_1, as shown in Fig. 11. The other intersection, point U in Fig. 11, is an unstable equilibrium point. Note that an unstable equilibrium cannot be observed in practice because the noise or environmental variations would cause the trajectory to diverge from the unstable equilibrium, even if it is possible to set up the exact initial conditions corresponding to this point [26].

With the addition of heat transfer in the exhaust manifold ($Ah_{\rm gw} = 2.5\,{\rm W/K}$), the slope of the breathing temperature curve (from $T_{\rm bd}$ to $T_{\rm ivc}$) increases as shown in Fig. 11. This slope change corresponds to a weaker cycle-to-cycle coupling of the temperature dynamics. Extremely high heat transfer case (high $Ah_{\rm gw}$) would result in a vertical breathing temperature curve and stop the internal feedback loop from $T_{\rm bd}$ to $T_{\rm ivc}$. In other words, $T_{\rm ivc}$ is only affected by the wall temperature T_w from (13) and (14). We conclude that the wall temperature and the heat management are very important to the operation of HCCI engines.

With better understanding of the heat transfer effect on the stability of HCCI engine, we can develop a better heat management strategy to provide enough heat required for autoignition and avoid instability. For instance, a controllable and fully integrated cooling system could be used to enhance the self-heating tendency at some operating points for fast warm-up strategies. On the other hand, we may have to cool down the exhaust manifold to avoid instability or early ignition at high loads.

V. Temperature Dynamic Trajectories

To generate the simple 2-D returning maps in Section IV, we neglected the intake and exhaust manifold filling dynamics and assumed that the equilibrium flow is achieved much faster than the equilibrium temperature. In this section, we use the full order model in [9] for an HCCI engine with insulated exhaust manifold to illustrate transitions between the identified temperature equilibria during critical load transitions. Recall from Section II-C that for an engine with insulated exhaust manifold, we have $T_{\rm rbl} = T_{\rm bd}$ at steady state. Thus, the y-axis of the steady-state temperature map can be replaced with $T_{\rm rbl}$. We demonstrate that nonoptimized sequences of the input command RBL can result in large temperature excursion that can damage the engine or lead to misfire. It is then shown in Section V-C that the dynamic (cancelation) feedforward controller presented in Section V-B can produce RBL commands that safely allow load transition between two stable equilibria.

A. Open-Loop Temperature Trajectories

During a fuel step, the temperature dynamic trajectory moves along the breathing line to the combustion curve of the next fueling level. As shown in Fig. 12, the trajectories move up and down the dash-dot line as fuel steps up from 9 to 10 mg/cycle and steps down from 10 to 9 mg/cycle, respectively. The transitions follow slightly different paths when fuel steps up and down due to the exhaust pressure and flow dynamics. On the other hand, the IVC temperature ($T_{\rm ivc}$) increases as RBL steps up, and similarly, drops as RBL steps down. After the manifold flow dynamics catches up, the trajectory follows the corresponding breathing line back to the combustion curve associated with the commanded fueling level, as shown in Fig. 12. The temperature trajectories follow different paths when RBL steps up and down. In particular, when RBL steps up from 3.6 to 4 mm, $T_{\rm ivc}$ increases immediately in the next cycle and then goes up along the breathing line till it intersects the combustion curve. On the other hand, when RBL steps down from 4 to 3.6 mm, $T_{\rm ivc}$ drops immediately in the next cycle and then goes down along the breathing line till it intersects the combustion curve.

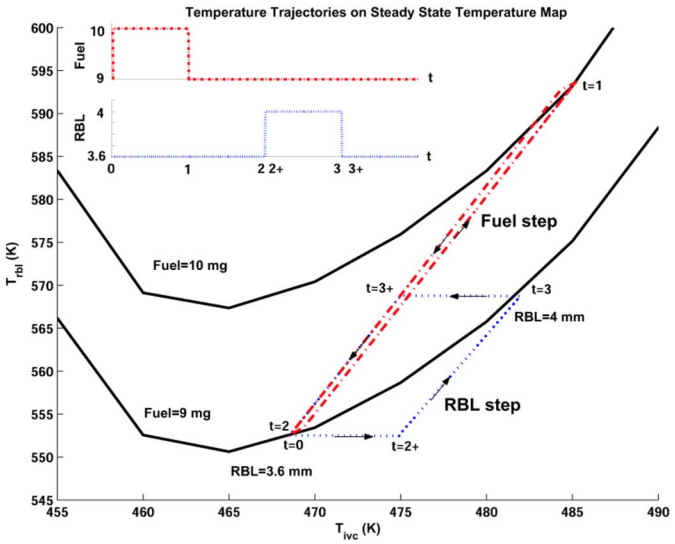

Fig. 12. Open-loop temperature trajectories for fuel steps 9 → 10 mg/cycle and 10 → 9 mg/cycle and RBL steps 3.6 → 4 mm and 4 → 3.6 mm. The trajectories follow different paths when fuel or RBL steps up and down.

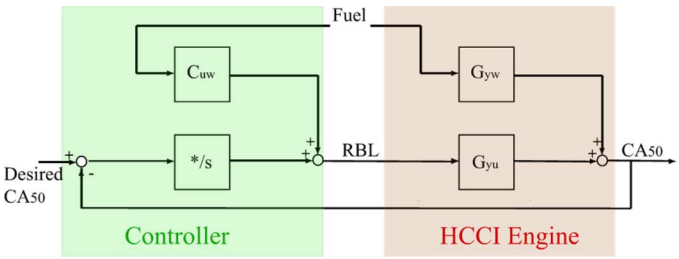

Fig. 13. Block diagram of the HCCI engine plant with a dynamic (cancelation) feedforward controller and an integral feedback controller.

B. Dynamic Feedforward Controller

Fig. 13 shows the linearized HCCI engine plant with a dynamic (cancelation) feedforward controller and an integral feedback controller. The HCCI engine plant is linearized around the equilibrium point of 9 mg/cycle fueling rate and 3.6 mm RBL. The input-output (I/O) behavior of the linearized plant can, thus, be represented by the transfer functions from Fuel and RBL to the combustion timing CA_{50} (crankangle for 50% fuel burned)

$$CA_{50} = G_{\rm yw} \cdot {\rm Fuel} + G_{\rm yu} \cdot {\rm RBL}. \tag{17}$$

Authorized licensed use limited to: IEEE Xplore. Downloaded on April 24, 2009 at 17:55 from IEEE Xplore. Restrictions apply.

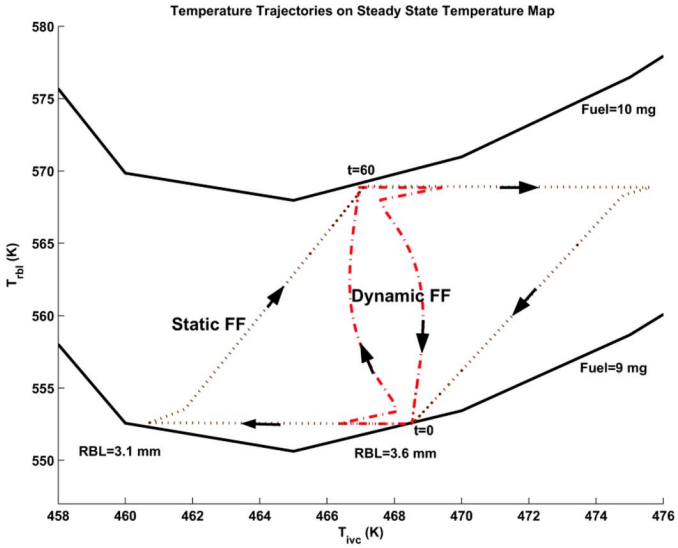

Fig. 14. Temperature trajectories with static and dynamic feedforward RBL controllers for fuel steps 9 → 10 mg/cycle and 10 → 9 mg/cycle. Both the static and dynamic feedforward RBL controllers are able to regulate the steady-state IVC temperature $T_{\rm ivc}$ to the optimum equilibrium point on each combustion curve, thus, regulating the combustion timing during the fuel step changes (times correspond to the time scale in Fig. 15).

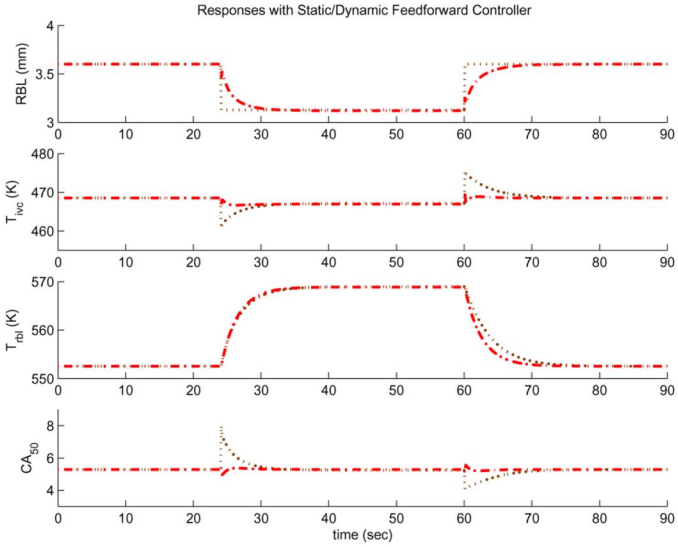

Fig. 15. Responses with static and dynamic feedforward RBL controller for fuel steps 9 → 10 mg/cycle and 10 → 9 mg/cycle. The dynamic feedforward RBL controller does a much better job regulating the combustion timing during transient.

A cancelation feedforward controller can be derived from the transfer functions $G_{\rm yw}$ and $G_{\rm yu}$

$$C_{\rm uw} = -G_{\rm yu}^{-1} G_{\rm yw}. \tag{18}$$

In practice, the plant transfer functions can be derived from a real time identification. In this paper, the plant transfer functions $G_{\rm yu}$ and $G_{\rm yw}$ are derived after linearization and balanced realization are applied to the normalized full order model. The resulting feedforward $C_{\rm uw}$ from Fuel to RBL is a fourth-order controller

$$C_{\rm uw} = \frac{-0.1466s^4 - 4.086s^3 - 29.22s^2 - 86.97s - 23.26}{s^4 + 36.63s^3 + 346.7s^2 + 229s + 38.35}. \tag{19}$$

The RBL command is augmented by an integral controller to avoid steady-state CA_{50} errors

$$\text{RBL} = C_{\rm uw} \cdot \text{Fuel} - \frac{0.3}{s} \cdot \left(CA_{50}^{\rm des} - CA_{50}\right). \tag{20}$$

C. Controlled Temperature Trajectories

Figs. 14 and 15 show the controlled performance with a static feedforward RBL controller and the dynamic feedforward RBL controller of (20) during fuel steps from 9 to 10 mg/cycle and from 10 to 9 mg/cycle. Fig. 14 shows that both the static and dynamic feedforward RBL controllers are able to regulate the steady-state IVC temperature $T_{\rm ivc}$ to the optimum equilibrium point on each combustion curve, thus, regulating the combustion timing during the fuel step changes. However, the transient IVC temperature excursions are bigger during the instantaneous step change in RBL commanded by the static feedforward controller

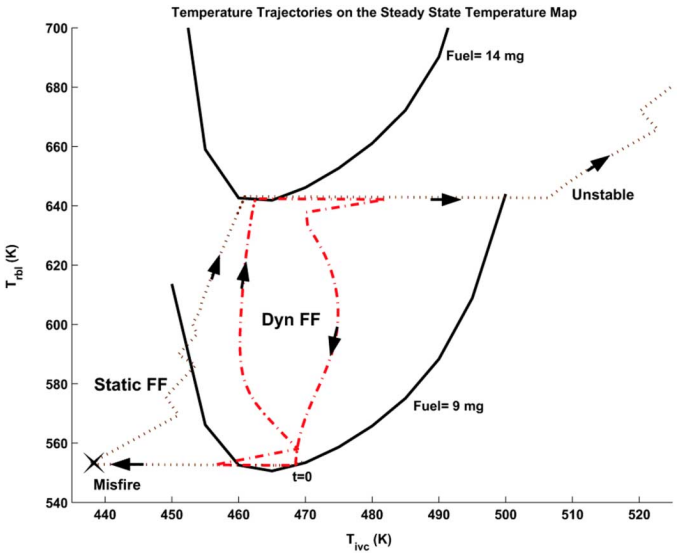

Fig. 16. Temperature trajectories with static and dynamic feedforward RBL controllers for fuel steps 9 → 14 mg/cycle and 14 → 9 mg/cycle. With static feedforward RBL controller, engine misfire occurs in the first cycle while fuel steps up and the engine temperature grows unbounded when fuel steps down.

as can be shown from both Fig. 14 and the $T_{\rm ivc}$ response in Fig. 15. On the other hand, Fig. 15 shows that, by changing RBL slowly, the dynamic feedforward controller improves the combustion timing regulation during transients.

Fig. 16 compares the performance with the static and dynamic feedforward controllers during larger fuel steps (from 9 to 14 mg/cycle and from 14 to 9 mg/cycle). The performance with the dynamic feedforward controller is still smooth and stable. The performance with the static feedforward controller, however, deteriorates substantially. First, engine misfire occurs in the first cycle while fuel increases from 9 to 14 mg/cycle. When fuel increases, the static feedforward controller issues a command to decrease RBL immediately. During the simultaneous

Authorized licensed use limited to: IEEE Xplore. Downloaded on April 24, 2009 at 17:55 from IEEE Xplore. Restrictions apply.

increase in fuel and decrease in RBL, misfire occurs due to the dramatic drop in T_{ivc}. Second, the engine temperature grows unbounded when fuel steps down from 14 to 9 mg/cycle. When fuel steps down, the static feedforward causes RBL to increase immediately, and as a consequence a lot of hot exhaust gas at this high fueling level (14 mg/cycle) is brought into the cylinder immediately. The hot charge advances the combustion timing and, thus, makes the exhaust gas even hotter, which further advances the timing. As can be shown from Fig. 16, the hot charge brings the temperature trajectory to the unstable region, as we discussed in Section IV and observed in [25].

VI. Conclusion

The existence of multiple steady-state temperature equilibria and their stability under different heat transfer conditions is analyzed in this paper. It is shown that the autoignition, which is based on high exhaust gas recirculation and, thus, strong cycle-to-cycle temperature coupling, can depart from the region of attraction of a stable equilibrium during large and fast changes in fueling level. We present a dynamic feedforward controller that is able to maintain stable transitions between two stable equilibria by reducing temperature excursions and, hence, keeping the temperature trajectories within stable regions. A static feedforward controller, on the other hand, can cause instability due to a nonoptimized transition from a hotter region (higher fueling level) to a cooler region (lower fueling level). Mode transition from SI to HCCI [27] or from CI to HCCI [28] can exhibit similar difficulties. With better understanding on the region of attraction of the multiple equilibrium points, a controller for the HCCI engine and SI/HCCI mode switching can be developed.

This work could be extended by including the effect of the composition on the combustion model [29] in an effort to explain the chemical coupling in addition to the dominant thermal coupling. Considering the effects of chemical energy coupling could be necessary in specific situations such as [16] 1) effect of $\mathrm{NO_x}$ in residuals on combustion timing in subsequent cycles and 2) where a partially burnt or a close-to-misfire cycle leads to fuel-rich mixture in the subsequent cycle leading to advanced autoignition.

Acknowledgment

The authors would like to thank General Motors Corporation for the experimental data.

References

[1] J. Willand, R.-G. Nieberding, G. Vent, and C. Enderle, "The knocking syndrome—Its cure and its potential," SAE International, Warrendale, PA, Tech. Rep. 982483, 1998.

[2] J. Chen and W. Stevens, "Autoignition and Control of Flameless Combustion," Dept. Energy, Sandia Nat. Labs., Livermore, CA, 2002, pp. 1–2.

[3] P. Najt and D. Foster, "Compression-ignited homegeneous charge combustion," SAE International, Warrendale, PA, Tech. Rep. 830264, 1983.

[4] J. O. Olsson, P. Tunestal, B. Johansson, S. Fiveland, R. Agama, M. Willi, and D. Assanis, "Compression ratio influence on maximum load of a natural gas fueled HCCI engine," SAE International, Warrendale, PA, Tech. Rep. 2002-01-0111, 2002.

[5] D. S. Stanglmaier and E. Roberts, "Homogenous charge compression ignition (HCCI): Benefits, compromises, and future engine applications," SAE International, Warrendale, PA, Tech. Rep. 1999-01-3682, 1999.

[6] R. H. Thring, "Homegeneous-charge compression-ignition (HCCI) engines," SAE International, Warrendale, PA, Tech. Rep. 892068, 1989.

[7] C. J. Chiang and A. G. Stefanopoulou, "Sensitivity analysis of combustion timing and duration of homogeneous charge cmpression ignition (HCCI) engines," in *Proc. Amer. Contr. Conf.*, 2006, pp. 1857–1862.

[8] J. Martinez-Frias, S. M. Aceves, D. Flowers, J. R. Smith, and R. Dibble, "HCCI control by thermal management," SAE International, Warrendale, PA, Tech. Rep. 2000-01-2869, 2000.

[9] D. J. Rausen, A. G. Stefanopoulou, J.-M. Kang, J. A. Eng, and T.-W. Kuo, "A mean-value model for control of homogeneous charge compression ignition (HCCI) engines," *ASME J. Dyn. Syst., Meas. Contr.*, vol. 127, no. 3, pp. 355–362, 2005.

[10] G. Shaver, J. Gerdes, P. Jain, P. Caton, and C. Edwards, "Dynamic modeling of residual-affected hcci engines with variable valve actuation," *ASME J. Dyn. Syst., Meas. Contr.*, vol. 127, no. 3, pp. 374–381, 2005.

[11] C. V. Heerden, "Autothermic processes—Properties and reactor design," *Ind. Eng. Chem.*, vol. 45, no. 6, pp. 1242–1247, Jun. 1953.

[12] R. Aris and N. R. Amundson, "An analysis of chemical reactor stability and control," *Chem. Eng. Sci.*, vol. 7, no. 3, pp. 121–131, Jan. 1958.

[13] F. G. Liljenroth, "Starting and stability phenomena of ammonia-oxidation and similar reactions," *Chem. Metallurgical Eng.*, vol. 19, no. 6, pp. 287–293, Sep. 1918.

[14] J. C. Kantor, "A dynamical instability of spark-ignited engines," *Sci.*, vol. 224, pp. 1233–1235, Jun. 1984.

[15] M. Kaneko, K. Morikawa, J. Itoh, and Y. Saishu, "Study on homogenous charge compression ignition gasoline engine," in *Proc. 5th Int. Symp. Diagnos. Modeling Combustion Internal Combustion Engines*, Nagoya, Japan, Jul. 2001, pp. 441–446.

[16] A. Bhave, M. Kraft, F. Mauss, A. Oakley, and H. Zhao, "Evaluating the EGR-AFR operating range of a HCCI Engine," SAE International, Warrendale, PA, Tech. Rep. 2005-01-0161, 2005.

[17] J. Hiltner, R. Agama, F. Mauss, B. Johansson, and M. Christensen, "HCCI operation with natural gas: Fuel composition implications," in *Proc. ASME: Int. Combustion Engine Technol. Conf.*, 2000, pp. 24–27.

[18] P. A. Caton, H. H. Song, N. B. Kaahaaina, and C. F. Edwards, "Strategies for achieving residual-effected homogeneous charge compression ignition using variable valve actuation," SAE International, Warrendale, PA, Tech. Rep. 2005-01-0165, 2005.

[19] A. Caton and W. H. Ray, "On the dynamic behavior of continuous stirred tank reactors," *Chemical Eng. Sci.*, vol. 29, pp. 967–985, 1974.

[20] R. A. Schimitz, "Multiplicity, stability, and sensitivity of states in chemical reacting systems—A review," *Adv. Chemistry*, vol. 148, pp. 156–211, 1976.

[21] J. B. Heywood, *Internal Combustion Engine Fundamentals*. New York: McGraw-Hill, 1988.

[22] J. C. Livengood and P. C. Wu, "Correlation of autoignition phenomena in internal combustion engines and rapid compression machines," in *Proc. 5th Int. Symp. Combustion*, 1955, pp. 347–356.

[23] H. Zhao, Z. Peng, and N. Ladommatos, "Understanding of controlled autoignition combustion in a four-stroke gasoline engine," *J. Automobile Eng.*, vol. 215, no. 12, pp. 1297–1310, Dec. 2001.

[24] N. J. Killingsworth, S. M. Aceves, D. L. Flowers, and M. Krstić, "A simple HCCI engine model for control," in *Proc. IEEE Int. Conf. Contr. Appl.*, 2006, pp. 2424–2429.

[25] C. J. Chiang and A. G. Stefanopoulou, "Steady-state multiplicity and stability of thermal equilibria in homogeneous charge compression ignition (HCCI) engines," in *Proc. 43rd IEEE Conf. Dec. Contr.*, 2004, pp. 1676–1681.

[26] H. K. Khalil, *Nonlinear Systems*. Englewood Cliffs, NJ: Prentice-Hall, 1996.

[27] H. Santoso, J. Matthews, and W. K. Cheng, "Managing SI/HCCI dual-mode engine operation," SAE International, Warrendale, PA, Tech. Rep. 2005-01-0162, 2005.

[28] C. Musardo, B. Staccia, M. Shawn, Y. Guezennec, and G. Rizzoni, "Supervisory control for nox reduction of an HEV with a mixed-mode HCCI/CIDI engine," in *Proc. Amer. Contr. Conf.*, 2005, pp. 3877–3881.

[29] X. He, M. T. Donovan, B. T. Zigler, T. R. Palmer, S. M. Walton, M. S. Wooldridge, and A. Atreya, "An experimental study of isooctane ignition delay times at HCCI operating conditions using a rapid compression facility," *Combustion Flame*, vol. 142, pp. 266–275, 2005.

Authorized licensed use limited to: IEEE Xplore. Downloaded on April 24, 2009 at 17:55 from IEEE Xplore. Restrictions apply.

Chia-Jui Chiang received the B.S. degree from the National Chung Hsing University, Taichung, Taiwan, in 1995 and the M.S. degree in mechanical engineering from the National Taiwan University of Science and Technology, Taipei, Taiwan, in 1997. He is currently pursuing the Ph.D. degree in mechanical engineering at the University of Michigan, Ann Arbor.

He was a Photo Lithography Equipment Engineer (1999-2001) at Taiwan Semiconductor Manufacturing Company (TSMC), Hsinchu, Taiwan. His research interests include modeling, stability analysis, and control of thermal systems, especially automotive propulsion systems.

Anna G. Stefanopoulou (SM'05) received the Diploma from the National Technological University of Athens, Greece, in 1991, the M.S. degree in naval architecture and marine engineering, a second M.S. degree in electrical engineering and computer science, and the Ph.D. degree from the University of Michigan, Ann Arbor, in 1992, 1994, and 1996, respectively.

Currently, she is a Professor in the Mechanical Engineering Department at the University of Michigan. She was an Assistant Professor (1998–2000) at the University of California, Santa Barbara, and a Technical Specialist (1996–1997) at the Scientific Research Laboratories at Ford Motor Company, Dearborn, MI. Her current research interests include control of advanced internal combustion engines and fuel cell power systems.

Authorized licensed use limited to: IEEE Xplore. Downloaded on April 24, 2009 at 17:55 from IEEE Xplore. Restrictions apply.